



Impact of surface melt and brine infiltration on fracture toughness of ice shelves

Emma Pearce¹, Oliver J Marsh¹, Thomas M Mitchell², Jukka Tuhkuri³, Elizabeth R Thomas¹, and Siobhan Johnson¹

¹British Antarctic Survey

²University College London

³Aalto University

Correspondence: Emma Pearce (emmear@bas.ac.uk)

Abstract. Ice shelves are heterogeneous composites of firn, meteoric ice, refrozen melt and brine-saturated ice. The properties and distribution of these elements control ice shelf response to stress and susceptibility to fracturing. Here, we quantify how surface-melt and brine infiltration modify the Mode I fracture toughness (K_{Ic}) of meteoric ice on the Brunt Ice Shelf (BIS), Antarctica. During the 2023/24 austral summer, we recovered a 37 m core sequence from meteoric infill ice near Halley VI, 5 where radar mapping shows continuous brine horizons at \sim 37 m depth and line scans indicate that the upper 37 m contain \sim 7% refrozen melt. We combined density, salinity, temperature and grain size measurements with semi-circular three-point bending tests on samples representing (i) meteoric ice, (ii) melt-modified meteoric ice, and (iii) brine-infiltrated meteoric ice. Our results show melt-modified samples are consistently tougher than melt-free meteoric ice, with K_{Ic} increases up to \sim 40%. This is despite their larger grain size, indicating densification dominates over grain-size effects. In contrast, brine-saturated 10 meteoric ice exhibits markedly lower K_{Ic} , by 14% - 34% relative to density-matched, brine-free meteoric ice, consistent with chemical weakening and lower freezing temperatures. Our results demonstrate that as K_{Ic} varies strongly with density, salinity and depth, a spatially and temporally constant toughness value is unlikely to reproduce calving behaviour accurately. Implementing spatially and vertically variable K_{Ic} values, and understanding how ice shelf structure and composition evolves 15 over time, is essential to improve predictions of rift propagation and calving.

15 1 Introduction

Antarctic ice shelves play an essential role in restraining the flow of inland glacier ice. They can be weakened by basal-melt-driven thinning (Pritchard et al., 2012) or surface-melt-induced hydrofracture leading to acceleration in the flow of grounded glacier ice (Scambos et al., 2004), and increasing the contribution to global sea level rise. The rapid collapse of the Larsen B Ice Shelf in 2002 serves as an example of this process, where following the disintegration of the ice shelf, inland ice 20 velocities quadrupled (Glasser and Scambos, 2008; Scambos et al., 2004).

Part of the natural cycle of ice shelf growth and deterioration in stable conditions is ice shelf rifting, where full-thickness fractures create tabular icebergs (De Rydt et al., 2019). Rifts nucleate from pre-existing weaknesses in the ice shelf, caused by the build-up of stress around pinning points or shear margins (Larour et al., 2004; Walker et al., 2013; Bassis et al., 2005;



Fricker et al., 2005a). Rift growth is episodic, with bursts of propagation occurring over hours to days and often accompanied by rapid widening and an increase in seismic activity (Fricker et al., 2005b, a). While rift paths broadly follow the principal extensional stress field set by the ice shelf geometry and flow direction (Larour et al., 2004; Walker et al., 2013), their timing and rate depend on both external forcing and local material properties (Borstad et al., 2017; Kulessa et al., 2019; Lipovsky, 2020).

To add complication to the rifting process, ice shelves are not made up of homogeneous ice; they are complex composites of firn, refrozen melt, meteoric ice, and marine ice, with mechanical properties that vary both spatially and with depth. Processes such as surface melting can introduce centimetre-thick melt layers that span hundreds of metres horizontally, increasing the density of the upper surface and reducing porosity. In extreme melt conditions, such as those caused by the high summer temperatures on the Larsen C Ice Shelf, melt ponding, and refreezing can introduce ice slabs up to 60 m thick within the firn (Hubbard et al., 2016). Brine infiltration adds further inhomogeneity and can, in particular, alter the mechanical character of ice, as saline pore-water reduces freezing temperature, enhances ductile failure, and promotes chemical weakening at grain boundaries (Cruz and Lipovsky, 2025). Marine suture zones, where brine and refrozen seawater are incorporated into the ice shelf, have been shown to be pervasive around the continent (Cook et al., 2018) and to both arrest rift propagation in some settings and enhance fracture in others, underscoring the highly variable role of brine in rift propagation (e.g., Kulessa et al., 2019; Borstad et al., 2017; Killingley et al., 2025).

In ice-fracture modelling, it is assumed that most rifts on ice shelves grow predominantly in Mode I (opening) under tensile or flexural-tensile stresses, and hence can be represented in two ways. Firstly by linear-elastic fracture mechanics, which treats rifts as cracks in a thin, elastic plate loaded by along-flow tension and by flexure from tides and waves, where propagation is dictated by the condition that the Mode I stress-intensity factor must exceed the local fracture toughness ($K_I \geq K_{Ic}$) (e.g., van der Veen, 1998; Lipovsky, 2020; Clayton et al., 2024). Secondly, by continuum-damage models that present rifting using an internal damage field that concentrates damage into rifts and reproduces observed spatial patterns of weakening. These approaches have been used to assess rift stability at the shelf-wide scale (e.g., Borstad et al., 2017, 2012; Krug et al., 2014; Huth et al., 2023).

Across both types of models, the key material parameter controlling the advance of the fracture is the Mode I fracture toughness, K_{Ic} (in the order of 100 kPa m^{0.5} for glacier/shelf ice), which sets the threshold for crack growth and therefore controls predicted rift initiation and the timing of calving (Rist et al., 2002; Lipovsky, 2018). Rift growth is a threshold process, excluding subcritical growth (Weiss, 2004; Atkinson, 1984), and as such, propagation can only occur once the stress intensity factor exceeds the maximum local K_{Ic} along the fracture path. This implies that rifts must accumulate sufficient elastic energy to overcome zones of high fracture toughness before they can advance, which explains their episodic growth behaviour (Van der Veen, 1998).

Laboratory and field measurements show that the fracture toughness of glacier ice (K_{Ic}) spans a wide but poorly constrained range, depending on microstructure and physical state, where fracture toughness has been shown to depend on temperature, density, grain structure, and environmental conditions (Schulson, 2001; Schulson and Duval, 2009; Rist et al., 2002). Classic laboratory tests on freshwater polycrystalline ice established the baseline mechanics where K_{Ic} typically lies between 100 -



300 kPa m^{0.5} at below zero temperatures, but decreases rapidly toward the melting point, where ice with values of \sim 300 kPa
60 m^{0.5} at -10°C can fall to \sim 200 kPa m^{0.5} near -5°C (Schulson, 2001; Rist et al., 2002; Dempsey, 1991).

Grain size exerts a strong control, with larger grains lowering toughness by facilitating inter-granular fracture, while finer
grains inhibit crack advance and promote higher K_{Ic} (Nixon and Schulson, 1987; Rist et al., 2002), with K_{Ic} decreasing from
~ 300 kPa m^{0.5} at grain sizes of \sim 1 mm to \sim 150 kPa m^{0.5} at grain sizes of 5–10 mm (Nixon and Schulson, 1987). Density
and porosity further control toughness, where shallow, porous firn can be as low as 50–100 kPa m^{0.5}, compared to compact
65 meteoric ice at depth, which can exceed 300 kPa m^{0.5} (Rist et al., 2002; Alley and Bentley, 1988). Previous work by Rist
et al. (1996, 2002) provided a foundational understanding of how fracture toughness varies with depth and microstructure in
an Antarctic ice shelf. Using three-point bend and uniaxial compression testing on ice cores from the Ronne Ice Shelf, they
found that apparent fracture toughness increases steadily through the firn and meteoric ice layers before plateauing in denser
70 ice. Their results demonstrated a strong positive correlation between K_{Ic} and density, with little to no dependence on grain
size once a sufficient number of grains were present across the specimen diameter. They also observed that brine-influenced
ice tends to exhibit lower and more variable toughness, potentially due to chemical weakening or inter-granular flaws.

Most existing measurements of K_{Ic} for glacier ice have been derived from clean, cold, meteoric ice, leaving uncertainty
for melt-affected or brine-infiltrated marine ice. Limited studies on chemical effects have been shown to lower K_{Ic} , as solutes
concentrate along grain boundaries and promote semi-liquid, inter-granular films that weaken cohesion (Cullen and Baker,
75 2001). Furthermore, laboratory tests on saline sea-ice similarly demonstrate that fracture toughness decreases with increasing
brine volume, with the associated reduction in freezing temperature driving additional weakening (Timco and Frederking,
1983).

Ice-shelf calving models often utilise idealised, constant toughness values across the whole ice shelf in the range of 100–200
kPa m^{0.5} for brittle fracture thresholds (e.g., Pralong and Funk, 2005; Albrecht and Levermann, 2012; Borstad et al., 2012;
80 Krug et al., 2014; Christmann et al., 2015), despite evidence that natural variability is far larger and that differences in ice shelf
composition can strongly influence ice shelf dynamics (e.g., Craw et al., 2023). Furthermore, as Antarctica warms, ice shelves
are projected to thin (Naughten et al., 2023), snow accumulation rates increase (Nicola et al., 2023), and melt events become
more common (Orr et al., 2023), hence ice shelves will develop increasingly heterogeneous structures dominated by firn, melt
and brine infiltration.

85 Since the 1990s, many ice shelves have thinned by tens of metres due to enhanced basal melting (Pritchard et al., 2012;
Adusumilli et al., 2020; Naughten et al., 2023), while episodic surface melt events and ponding have intensified in regions
of the Antarctic Peninsula and West Antarctica (Scambos et al., 2009; Wille et al., 2022). Crack initiation and propagation
thresholds on ice shelves should be expected to be neither spatially uniform nor constant through time, and will consist of an
array of toughness values controlled by grain size, density, temperature, porosity, and impurity content.

90 In this study, we directly quantify how re-frozen surface–melt and brine infiltration modify the Mode I fracture toughness (K_{Ic}) of ice from the Brunt Ice Shelf (BIS). We extend previous laboratory results (e.g., Rist et al., 1996, 2002) by
directly contrasting refrozen melt with brine infiltration in meteoric ice of similar density. This isolates the competing effects



of melt-driven densification versus brine-induced weakening, providing the first controlled dataset to quantify both processes in Antarctic shelf ice.

95 2 Brunt Ice Shelf

The Brunt Ice Shelf (BIS) is situated along the Eastern coast of the Weddell Sea, flowing north-west from the Caird Coast of Coats Land. It forms the southernmost section of a complex ice shelf system made up of the Stancomb-Wills Glacier Tongue and the Riiser-Larsen Ice Shelf to the East (Figure 1).

The BIS exhibits a heterogeneous structure resulting from its unique formation processes. As ice flows off the continent over 100 a steep grounding zone, it undergoes extensive crevassing, leading to the fragmentation of the ice into large blocks measuring between 2,500 and 6,000 metres in length and 250 to 900 metres in width (King et al., 2018). These blocks, composed primarily of dense continental ice, are interspersed with zones of sea ice, creating a mosaic-like structure. Accumulated snowfall and drifted snow fills the surface depressions between the blocks, smoothing the surface topography. Ground Penetrating Radar (GPR) data have found the thickness of the ice shelf to vary between the thick (approximately 250 m) continental ice blocks 105 interspersed with the thinner (approximately 150 m) sections of sea and meteoric infilled ice (King et al., 2018). Hereafter we refer to the mix of infilled compressed snow and sea ice as ‘infilled’ ice.

Due to the porous and permeable nature of the infilled ice sections, seawater (brine) can propagate through these areas and reach the height of sea level (approximately 30 - 40 m below the surface), leading to brine-saturated ice below this level. The 110 brine infiltrates when isostatic loading by snow accumulation on the sea ice layers pushes the sea ice below sea level. Since the firn has not fully consolidated to pore close-off, it is still porous and permeable, allowing seawater to infiltrate. Radar mapping shows that the BIS has these continuous brine layers within the infilled ice, disappearing in the more dense, impermeable continental ice blocks (King et al., 2018) (Figure 1). Analogous surveys on the McMurdo and Larsen C Ice Shelves confirm the same radar signature of brine (Grima et al., 2016; Killingbeck et al., 2025).

Over the past five years, two major rift systems, Chasm 1 and Halloween Crack, have developed on the BIS, culminating in 115 the calving of two large tabular icebergs: A-81 in January 2023 and A-83 in February 2024. Following the calving of iceberg A-81, the ice shelf’s flow speed increased from an average of 1–2.5 metres per day to approximately 4 metres per day, attributed to the loss of buttressing provided by the McDonald Ice Rumples (Marsh et al., 2024). As both these rifts progressed, they preferentially followed the zones of infill ice, while frequently slowing or arresting at the denser blocks of continental ice.

The interplay between the BIS’s structural composition and rift dynamics underscores the importance of understanding 120 the mechanical properties of its constituent ice types. Investigating how features like melt layers and brine infiltration affect fracture toughness is crucial for improving predictive models of ice shelf stability and potential contributions to sea-level rise.

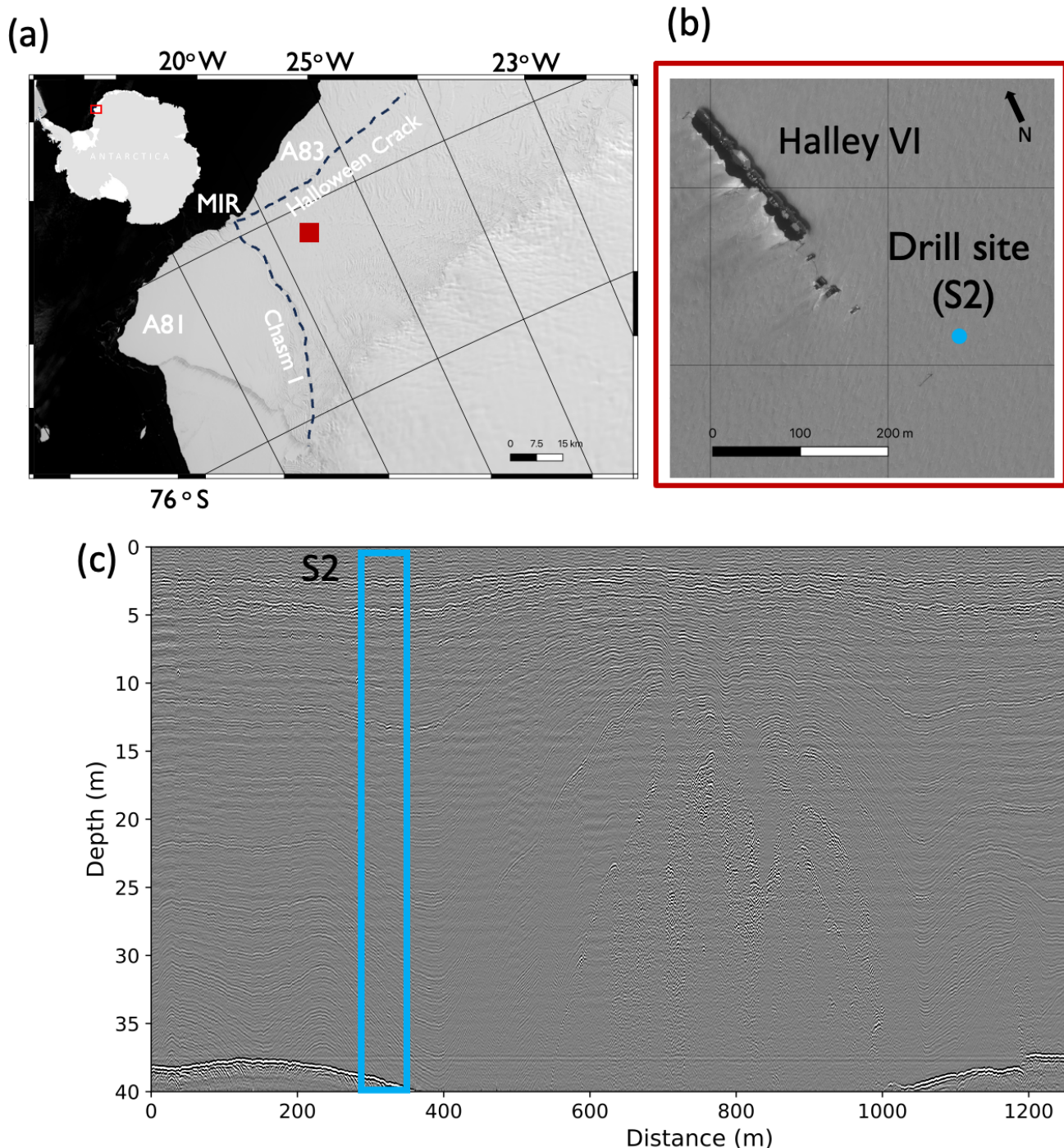


Figure 1. (a) The location of the Brunt Ice Shelf in East Antarctica and the McDonald Ice Rumples (MIR), which acts as a grounded pinning point for the ice shelf. (b) The location of the drill site, S2, next to the British Antarctic Survey's Halley VI research station. (c) GPR data acquired to locate a block of continental ice and the infilled ice. Brine infiltrates to a depth of approximately 37 m in the permeable infilled ice. The continental ice block shows no brine infiltration. Isochrones in the GPR data highlight annual layering, with brighter reflections linked to visible melt layers observed in the cores.



3 Data and Method

During the 2023/2024 Antarctic summer season, ice cores were recovered from a 37 m borehole drilled close to the site of Halley VI research station (Figure 1). Data were collected from the infilled ice (site S2), to establish variations in ice properties 125 and the controls these have on fracture toughness of the 'weaker' ice type. The borehole site was located using GPR data to ensure cores were collected from an area where brine infiltration was present.

3.1 Ice core recovery and borehole measurements

A medium-depth mechanical ice core drill (Mulvaney et al., 2002) was used to recover a continuous ice core record. Each core section was approximately 105 mm in diameter, with lengths up to 90 cm, although section length varied during drilling. 130 Drilling was stopped at 37 m depth after two days when brine infiltration saturated the ice and prevented further drilling progress.

As cores were recovered, they were measured and weighed to obtain an average density with depth. Once ice core recovery was finished, seven TinyTag temperature loggers were placed at 2.5 m intervals down the borehole and left overnight (Figure 2). The loggers were then raised by 2 m and left for a further 3 hours to obtain additional temperature measurements. 135 Ice cores were returned to the UK by the RRS Sir David Attenborough, being kept at a constant temperature of -20°C. They were then stored at the British Antarctic Survey's ice core facility, remaining at -20°C.

3.2 Line Scan

Ice cores were pre-processed by cutting the cores in half lengthwise. One-half of the cores were line-scanned to enable the identification of melt. Melt thickness was calculated by measuring the depth of the top and bottom of a continuous melt layer. 140 The total melt within the 37 meters of collected core equated to 2.47 m, 6.68% (Figure 2b).

3.3 Thin Sections

Thin sections were prepared to assess the ice crystal structure and grain size of the meteoric infilled ice and the melt inclusions. Two thin sections were prepared from core 35. Each thin section was cut from a single slice of ice at a uniform depth, ensuring that all crystals within the section originated from the same depth interval. The ice surface was levelled with a band saw and 145 mounted onto a glass plate using water at 0°C, then thinned with a microtome to a thickness less than one grain-size. The sections were examined on a light box under cross-polarised light to determine grain size and crystal structure (Figure 3). Both sections exhibited isotropic crystal fabrics. The section without visible melt features had an average grain size of 1 mm, whereas the melt-affected section displayed larger grains (5–10 mm).

3.4 Salinity measurements

150 Measurements were obtained from discrete ice samples cut from cores 41, 42, 43 and 44. Segments cut for salinity determination were melted in sealed glass jars and the meltwater was analysed using a SciQuip Precision SQ-7071 conductivity and

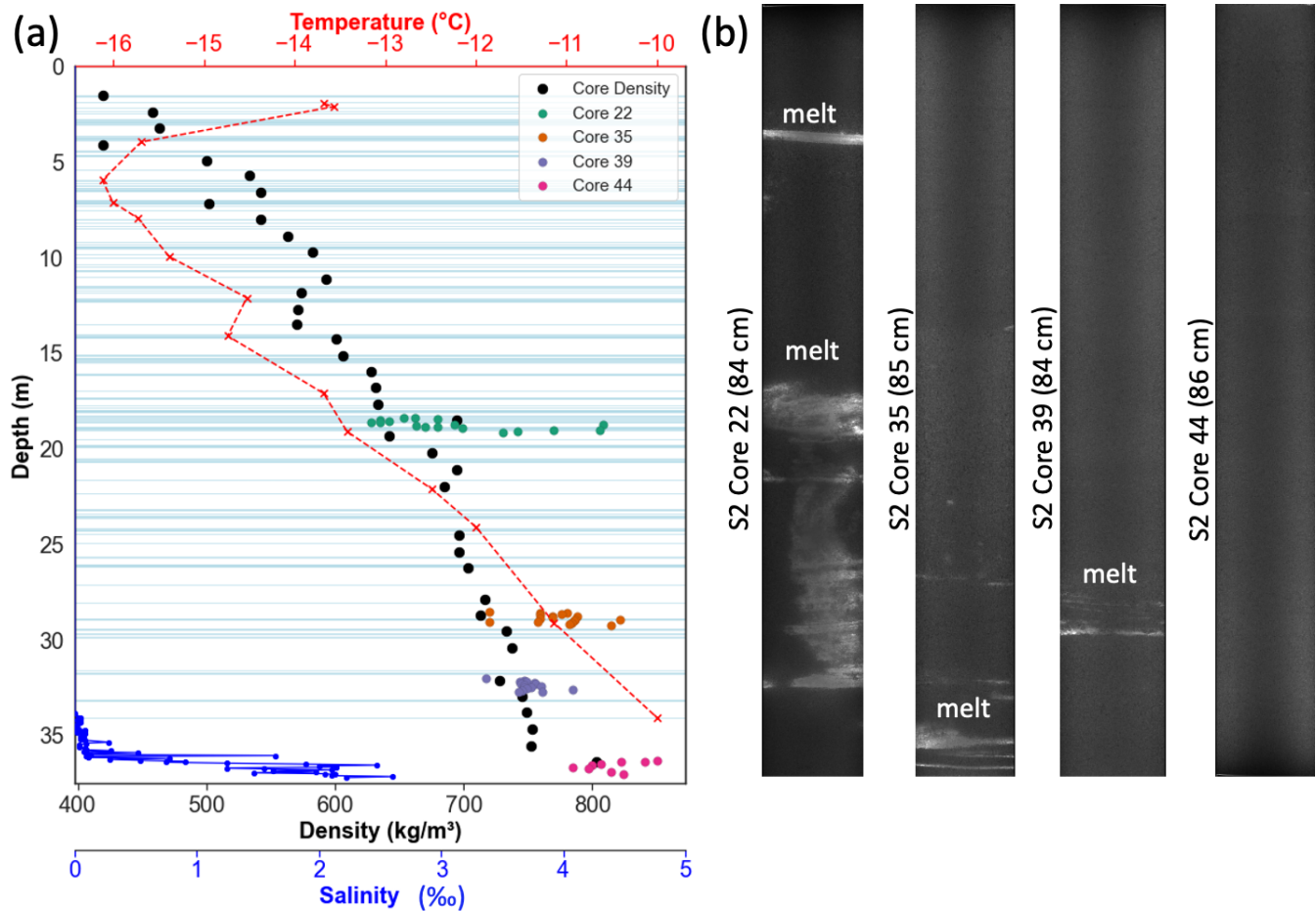


Figure 2. (a) Density measurements for whole cores (black) measured in the field, and smaller samples cut from the same cores used for fracture analysis (green, orange, purple, pink) measured in the lab. The spread in density from core samples is reflective of the melt within the cores, where the presence of melt layers in the cores is shown by the background blue bands. Red dashed line shows temperature data recorded at specific depth intervals using TinyTag loggers. (b) Line-scanned cores for core 22 (with a top depth of 16.45 m), 35 (27.67 m), 39 (31.07 m) and 44 (35.92 m). Line scan data highlight the melt within the cores.

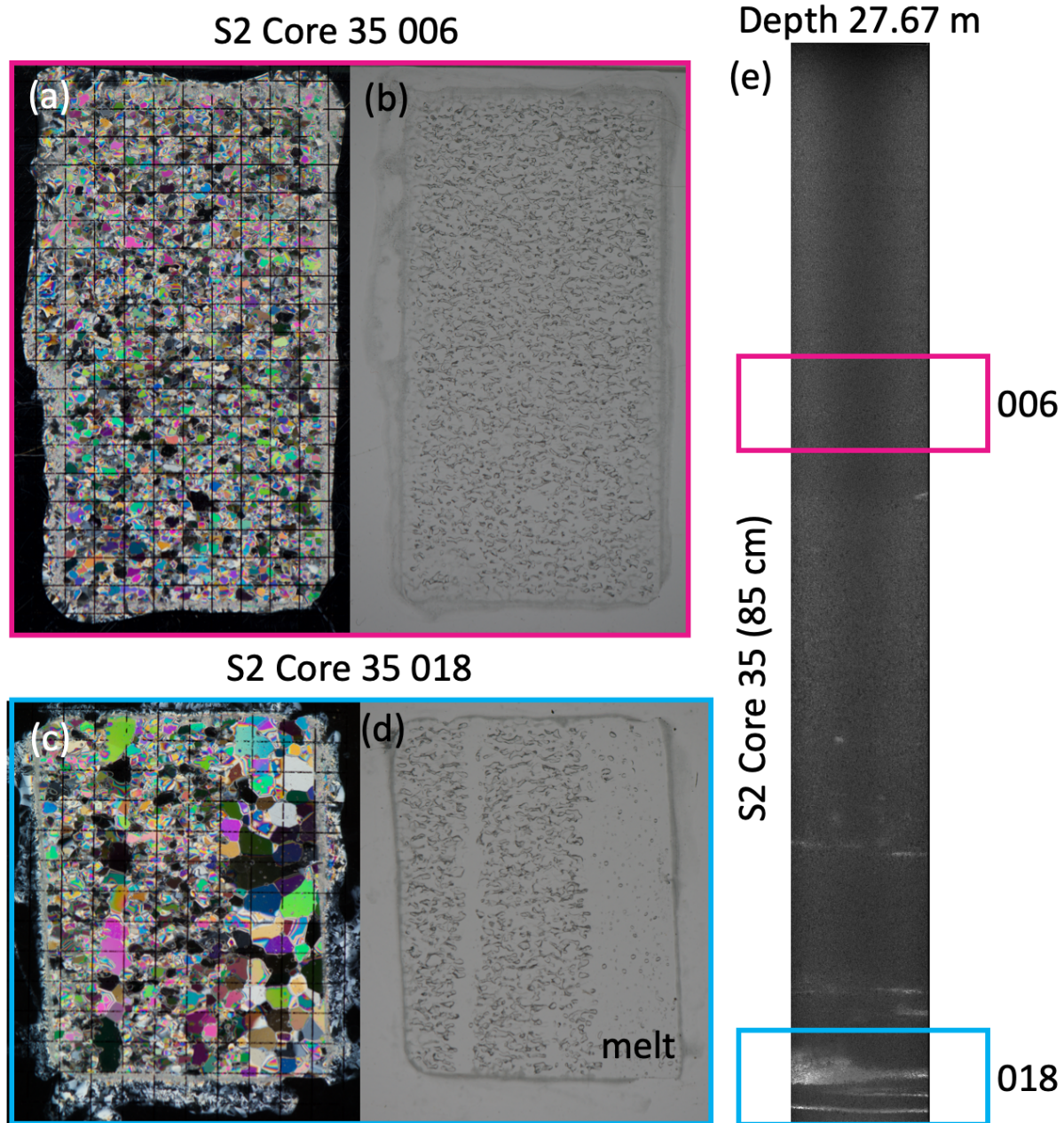


Figure 3. (a) a 5 mm grid overlaid on a thin section under polarised light taken from core 35, sample 006 of meteoric, infilled ice with no melt present. (b) The thin section sample with no polarised light. (c) Thin section taken from sample 018 of the same core, with the presence of a melt layer shown under polarised light. The melt layer exhibits larger grain size and fewer bubbles than the surrounding ice. (d) The thin section with the melt is shown under normal light. (e) Core 35 from which the thin sections are taken.



temperature meter. This instrument has a reported accuracy of 0.5% of its maximum measurement range for conductivity and 0.5°C for temperature. The practical salinity (PSS-78) of the samples was calculated using the relationship between pressure, temperature and conductivity as outlined in Lewis (1980).

155 The salinity of the Weddell Sea is approximately 35‰ (Foster and Carmack, 1976). Our values (Figure 2a), show an average salinity of between 0.2‰ and 0.8‰ for samples above 35 m, reaching a maximum salinity of 2.2‰ at the bottom of the borehole, at approximately 37 m depth.

3.5 Ice Fracture Samples

160 Four cores were selected to run fracture analysis tests on: cores 22, 35, 39 and 44. The cores were chosen due to their differing densities, melt inclusion and the presence of brine saturation (Core 44), enabling a wide span of fracture toughness measurements to be obtained. Each core produced between 9 to 17 samples by following the method of Kuruppu et al. (2014). Semi-circular samples were prepared for use with a three-point bending test to determine the Mode I static fracture toughness of the ice (Figure 4).

165 The sample's diameter is related to the average grain size in the ice by a ratio of at least 10:1, and the minimum sample thickness is the larger of 0.4D or 50 mm (Table 1).

Table 1. Dimensions of the SCB specimen. The dimensions were selected based on the work by Kuruppu et al. (2014)

Variable	Criteria	Size (mm)
T	$T \geq 0.4D$	42
D	$D \geq 10 \times \text{grain size}$	105
a	$0.4 \leq a/R \leq 0.6$	26
S	$0.5 \leq S/D \leq 0.8$	80

170 The samples were stored and prepared at -15 °C using a band saw to cut the semi-circles perpendicular to the core long axis. Once the samples were of the correct thickness and diameter, they were weighed to get an accurate sample density (Figure 2). A notch was then cut into the samples using a thin cutting blade. Before fracturing, the notch tip was scored with a very thin blade to ensure the notch tip was less than the average grain size of the sample. The thickness (T) and radius (R) of each sample were measured four times to the closest millimetre. The notch length (a) was also measured four times after the samples were fractured, to ensure as accurate a reading as possible. If the sample had the presence of melt, the surface area of melt on the fractured surface was measured post-breaking of the sample, and a melt percentage was given for that sample.

175 The fracture tests were performed using a compressive hydraulic test system with the facilities to record the load and axial displacement. The load application is performed via a conventional three-point bend fixture, with the sample placed on two cylindrical rollers. The sample is then loaded at a constant displacement rate of 0.01 mm s⁻¹, with the displacement and the load recorded at 200 Hz. Our experimental approach includes refined fracture testing using a semi-circular bend specimen (SCB). This setup is particularly sensitive to differences in fracture behaviour in low-density samples such as firn, enabling

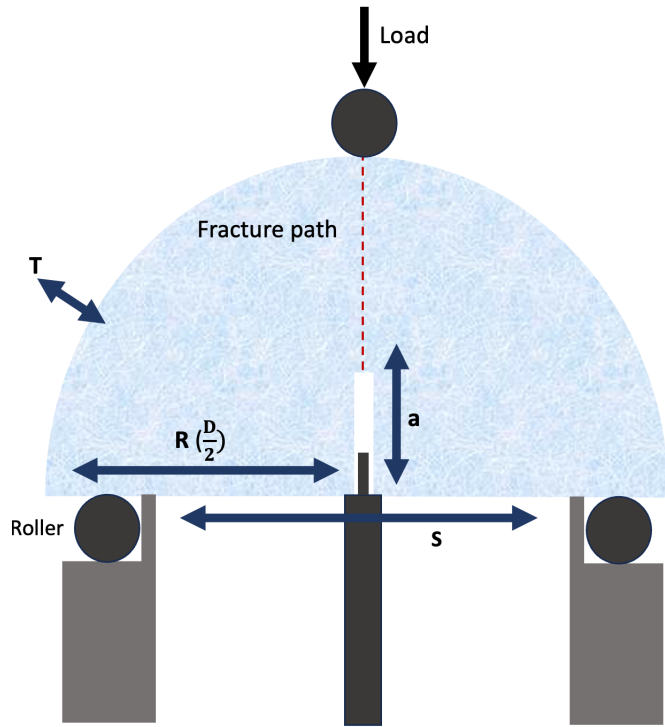


Figure 4. Experiment set up for ice fracture tests with semi-circular bend specimen. Dimensions used for the experiments can be found in Table 1.

more precise measurement of crack initiation and propagation, and offers tighter control over notch geometry and crack length than the three-point bending tests previously used on Antarctic shelf ice (e.g., Rist et al., 1996). This makes it especially 180 effective for detecting toughness contrasts introduced by melt inclusions or brine. All samples were stored and prepared at -15 °C. Experiments were conducted as quickly as possible in a room where temperatures fluctuated between -10 and -15 °C at the University College London cold room facilities.

4 Results: Fracture Toughness

Following the work of Kuruppu et al. (2014), mode I fracture toughness (K_{Ic}) of a sample, of thickness T can be calculated 185 using the peak force (P_{max}) as,

$$K_{Ic} = Y' \frac{P_{max} \sqrt{\pi a}}{2RT} \quad (1)$$

where Y' , the non-dimensional stress intensity factor assuming plane-strain conditions, can be calculated as;

$$Y' = -1.297 + 9.516(S/2R) - (0.47 + 16.457(S/2R))\beta + (1.071 + 34.401(S/2R))\beta^2 \quad (2)$$

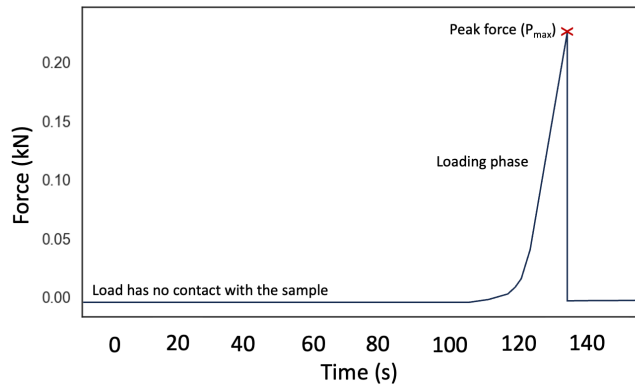


Figure 5. Loading phase from a three-point bending experiment on an ice core sample, where the peak force is used in the calculation of the Mode I fracture toughness.

where S represents the distance between the rollers, R the radius of the sample, and $\beta = \frac{a}{R}$ (as described in Figure 4 and 190 Table 1).

A Monte Carlo simulation is used to calculate the uncertainty in fracture toughness with the range of measured radius, thickness and crack length, to include a representative error in the values measured, due to the sensitivity of the method to the sample dimensions, with results from all cores shown in Figure 6.

In cores 22 and 39, for which both “no-melt” and “melt” data are available, the presence of melt is associated with an 195 increase in mean fracture toughness (Figure 6a). In core 22, the average fracture toughness rises from $76.7 \pm 12.2 \text{ kPa m}^{0.5}$ to $106.5 \pm 24.9 \text{ kPa m}^{0.5}$, representing an increase of nearly 39%. Core 39 shows a gain from $107.2 \pm 16.1 \text{ kPa m}^{0.5}$ to $130.8 \text{ kPa m}^{0.5}$, a 22% increase. This strengthening occurs irrespective of the increase in grain size associated with melt, which would traditionally lead to a reduction in toughness when larger grains are present. This demonstrates that the reduction in pore space and the associated increase in density due to melt refreezing plays a greater role in controlling fracture toughness than grain 200 size.

By contrast, core 35 exhibits a slight decrease in mean toughness upon melting, from $112.7 \pm 25.6 \text{ kPa m}^{0.5}$ without melt to $108.2 \pm 10.7 \text{ kPa m}^{0.5}$ with melt, a 4% reduction, well within the combined uncertainty of both groups. This non-significant drop may reflect natural variability in the limited melt-exposed subset, but it does not undermine the broader trend of melt-related toughening observed in the other cores.

205 Within core 22, the lowest density core, melt had a consistent positive effect, where even small melt fractions of $\sim 0.5\text{--}1\%$ increased toughness compared to melt-free samples. By contrast, in the higher-density cores of 35 and 39, the effect of melt was muted, with toughness values of melt-bearing and melt-free samples overlapping.

Fracture toughness in our dataset shows an expected strong baseline dependence on density, where fracture toughness increases systematically in core 22, 35 and 39 (Figure 6 b), showing that in these experiments, a key control on fracture toughness 210 is the reduction in porosity and increase in density. This is further supported by how the melt infiltration and refreezing consol-

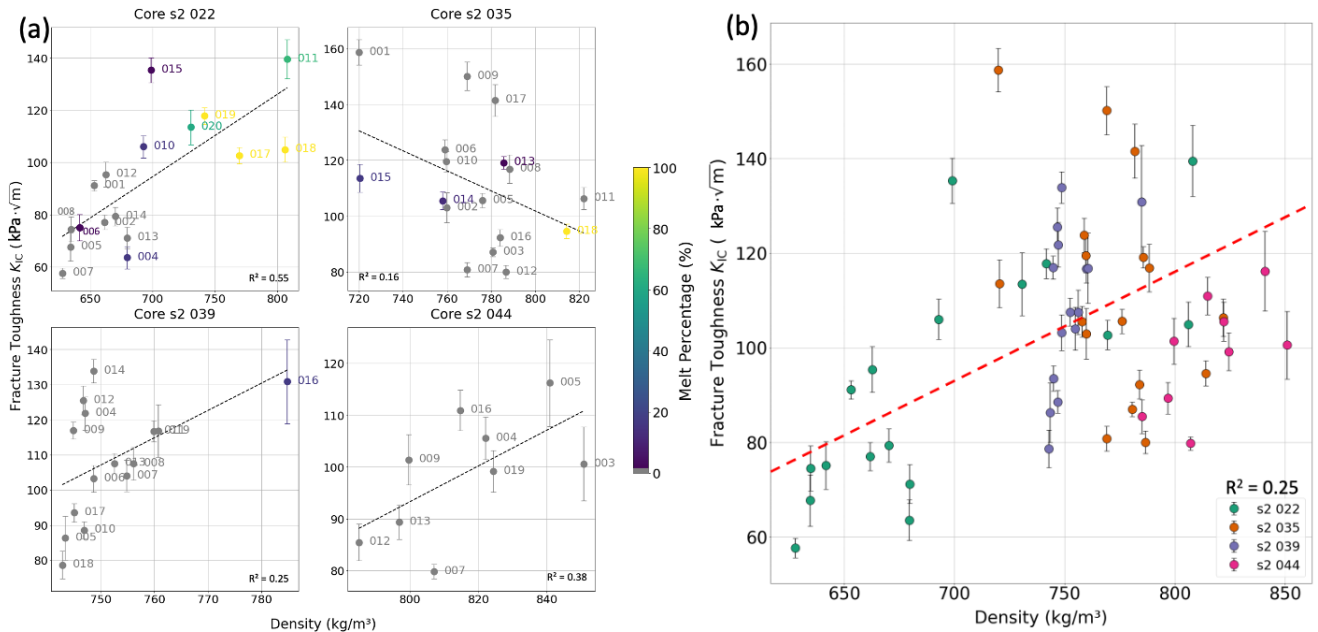


Figure 6. (a) Fracture toughness measurements from individual cores versus density. Colour indicates the percentage of melt on the fracture surface, where blue indicates no melt, and yellow 100% melt. (b) All fracture toughness values from all four cores versus density, where colour indicates the core.

imide the firn: in core 22 density rises from $654.4 \pm 17.2 \text{ kg m}^{-3}$ to $708.7 \pm 76.9 \text{ kg m}^{-3}$, in core 35 from $734.2 \pm 16.1 \text{ kg m}^{-3}$ to $749.2 \pm 46.1 \text{ kg m}^{-3}$, and in core 39 from $716.9 \pm 47.7 \text{ kg m}^{-3}$ to 786.6 kg m^{-3} .

Core 44 departs from this pattern, where despite having the highest mean density of all cores ($824.1 \pm 29.4 \text{ kg m}^{-3}$), its fracture toughness remains comparatively low ($98.7 \pm 11.9 \text{ kPa m}^{0.5}$). When compared against brine-free cores of the same density, core 44 samples are systematically weaker by 14%-34%, ($20-40 \text{ kPa m}^{0.5}$). We interpret this discrepancy as a consequence of the brine saturation within the samples. With an average salinity of 2.2‰, liquid brine in the pore spaces reduces the intergrain strength, lowers the freezing temperature, and therefore undermines the toughening normally imparted by densification. This weakening is consistent with a decrease in sea ice strength with an increase in brine volume(Weeks, 2010) and with observations of environmentally assisted crack growth in other brittle materials (Atkinson, 1984).

220 5 Discussion

Our experiments demonstrate that fracture toughness in ice shelves varies spatially and with depth. We identify two key processes that are responsible for some of this variability: the inclusion of melt layers and brine saturation. Refrozen melt consistently raises K_{Ic} in meteoric ice (by up to $\sim 40\%$), with a greater impact in the shallow firn, whereas brine infiltration reduces K_{Ic} by 14% - 34% relative to density-matched, brine-free meteoric ice. Refrozen melt is common on ice shelves, and



225 will become more prevalent in the future, as climate projections indicate greater melt potential and more extreme events (Orr
et al., 2023; Kittel et al., 2020; Noël et al., 2023). Brine infiltration occurs when firn at the water line is below sea level, which
may also become more common due to ice shelf thinning. Our results demonstrate that as K_{Ic} varies strongly with density,
salinity and depth, a spatially and temporally constant toughness value in ice shelf calving models is unlikely to accurately
reproduce patterns and timing of ice shelf calving, as theory already shows that including realistic variable, vertical properties
230 can alter predicted crevasse penetration depths by a factor of two (Clayton et al., 2024).

Our results are consistent with the observation that rifts on the Brunt Ice Shelf accelerate upon reaching zones of brine-
saturated infilled ice (lower fracture toughness), with fracture pathways that don't follow the preferential stress direction. Other
differences in properties may also play a role, including spatial variations in temperature profile, density profile and overall
235 thickness. It is not possible to assess the ice-shelf wide impact of melt layering, as melt layers are more difficult to quantify
spatially and to correlate with crack location. The thickness of the Brunt Ice Shelf makes it relatively sensitive to changes in the
firn, and it has already demonstrated its sensitivity to structural changes and external forcing (Marsh et al., 2024, 2025). These
laboratory-derived thresholds complement the recent finding that tidal flexure can act as a trigger for rift growth and calving
on the Brunt, highlighting how external stresses interact with internal heterogeneity: tides and hydrostatic stresses provide the
loading, while melt and brine determine the resistance. Additionally, the BIS temperature profile, with values of around -16°C
240 at the surface warming to -10°C at 37 m depth, sits close to the regime where fracture toughness decreases rapidly toward
the melting point. These relatively warm conditions at the brine layer would enhance the weakening effect of the brine. Thus,
as accelerated flow enhances ice shelf thinning on the BIS, the balance between melt-driven strengthening and brine-driven
weakening will increasingly dictate how rifts evolve.

Beyond the Brunt, many other Antarctic ice shelves are undergoing rapid change as a consequence of enhanced basal melt,
245 leading to ice shelf thinning and a larger influence of brine-saturated ice. The Amundsen Sea sector is a strong example, where
ice shelves have thinned substantially due to ocean-driven melting (Gudmundsson et al., 2019; Pritchard et al., 2012; Reed
et al., 2024). Along this coastline, incursions of warm modified Circumpolar Deep Water into ice shelf cavities drives some
of the highest basal melt rates observed in Antarctica, averaging 14–27 m yr^{-1} (Jacobs et al., 1992; Dutrieux et al., 2014;
Adusumilli et al., 2020; Reed et al., 2024). As a result, ice shelves in this sector (e.g. those from Pine Island (Dutrieux et al.,
250 2014) and Thwaites (Miles et al., 2020)) have thinned by tens to hundreds of metres over the past three decades. As thickness
declines, the relative influence of the firn and brine horizons in dictating the fracture resistance increases (Cook et al., 2018).
As basal thinning enhances the potential for brine infiltration to extend higher into still-permeable firn, as documented on the
Brunt and McMurdo ice shelves, this will create weak horizons along which rifts can propagate at accelerated rates (King et al.,
2018; Grima et al., 2016).

255 Our results show that near-surface melt and refreezing processes can alter K_{Ic} by tens of $\text{kPa m}^{0.5}$, and that the fracture
toughness of firn is not solely governed by grain size or depth, but is strongly modulated by the presence and state of melt.
In the shallowest samples (e.g., core 22), we observe that refrozen melt leads to a substantial increase in fracture toughness
(up to 40% higher than adjacent firn without melt inclusions). This effect appears to stem from localised densification as
meltwater fills and refreezes within the pore space, counteracting the expected weakening from larger grain sizes. However,



260 this strengthening effect diminishes in denser firn at depth, where the additional density from melt becomes proportionally smaller.

Ice shelves such as Larsen C already contain refrozen melt slabs tens of metres thick (Hubbard et al., 2016), which locally increase K_{Ic} but remove firn air content, reducing the capacity of the firn to buffer future melt and promoting ponding. The effect of melt therefore has two possible outcomes. Firstly, such ponding preconditions ice shelves for hydrofracture, the 265 mechanism implicated in the disintegration of Larsen A and B (Scambos et al., 2004). Secondly, melt-induced slab formation may act to temporarily strengthen the ice and alter how rifts propagate by increasing near-surface fracture toughness.

Together, our findings suggest that future ice shelves will comprise a combination of melt-strengthened and brine-weakened ice, with neighbouring units differing in fracture toughness by at least a factor of two. These opposing processes exert controls 270 on rift propagation, meaning that rift trajectories can be controlled by both local material heterogeneity and large-scale stress fields. By providing the first direct measurements of how melt and brine modify K_{Ic} , our study highlights the need for models to incorporate this variability when projecting rift initiation, propagation, and possible ice shelf collapse. Importantly, these results show that ice shelf fracture is not only controlled by geometry and external stresses but also by climate-driven processes that operate in the upper tens of metres of the firn. Future modelling efforts will need to account for the competing influences of refrozen melt and brine infiltration to accurately capture calving thresholds.

275 6 Conclusions

This study provides the first direct measurements of how refrozen surface melt and brine infiltration modify the fracture 280 toughness of meteoric ice from the Brunt Ice Shelf. Laboratory tests show that refrozen melt layers systematically increase K_{Ic} by reducing porosity and increasing density in the firn, with toughness gains of up to approximately 40%. In contrast, brine infiltration reduces K_{Ic} by 14–34 % relative to density-matched meteoric ice, reflecting chemical weakening at grain boundaries and lowered freezing temperatures. Together, these results demonstrate that fracture toughness in ice shelves is 285 neither spatially nor vertically consistent, but varies strongly with density, chemistry and porosity. More broadly, our results highlight how the future stability of the Brunt Ice Shelf, and of Antarctic ice shelves in general, will be governed not just by geometry and stress regime, but by the fine-scale, climate-driven heterogeneity of their structure. Our findings demonstrate that refrozen melt and brine infiltration can shift K_{Ic} by tens of $\text{kPa m}^{0.5}$ in opposite directions, even within adjacent ice units. This highlights the importance of incorporating vertical and horizontal variability in toughness into rift and calving models, so that 290 forecasts of ice shelf response to future warming can better capture the competing influences of melt strengthening and brine weakening.

Author contributions. EP and LT collected the ice cores in the 2023/2024 Antarctic season. EP, TM, and JT performed the ice fracture experiments and fracture toughness calculations. OM acquired the project funding. SJ produced the salinity measurements. EP wrote the 290 manuscript and OM, TM, JT and SJ contributed to edits and revisions.



Competing interests. The authors declare that they have no conflict of interest.

Acknowledgements. This research was supported by the Natural Environment Research Council (NERC, grant number NE/X014991/1). Fieldwork and ice core collection was made possible by the dedicated efforts of the British Antarctic Survey's Halley VI operations team and drill engineers during the 2023/24 season. We thank Shaun Miller for assistance with ice preparation and line scanning. JT was supported by 295 the Research Council of Finland (decision number 351229). We also acknowledge the use of ChatGPT (OpenAI, <https://chat.openai.com>) for assistance with Python code development and manuscript editing.



References

Adusumilli, S., Fricker, H. A., Medley, B., Padman, L., and Siegfried, M. R.: Interannual variations in meltwater input to the Southern Ocean from Antarctic ice shelves, *Nature geoscience*, 13, 616–620, 2020.

300 Albrecht, T. and Levermann, A.: Fracture field for large-scale ice dynamics, *Journal of Glaciology*, 58, 165–176, 2012.

Alley, R. B. and Bentley, C. R.: Ice-core analysis on the Siple Coast of West Antarctica, *Annals of Glaciology*, 11, 1–7, 1988.

Atkinson, B. K.: Subcritical crack growth in geological materials, *Journal of Geophysical Research: Solid Earth*, 89, 4077–4114, 1984.

Bassis, J., Coleman, R., Fricker, H., and Minster, J.: Episodic propagation of a rift on the Amery Ice Shelf, East Antarctica, *Geophysical Research Letters*, 32, 2005.

305 Borstad, C., Khazendar, A., Larour, E., Morlighem, M., Rignot, E., Schodlok, M., and Seroussi, H.: A damage mechanics assessment of the Larsen B ice shelf prior to collapse: Toward a physically-based calving law, *Geophysical Research Letters*, 39, 2012.

Borstad, C., McGrath, D., and Pope, A.: Fracture propagation and stability of ice shelves governed by ice shelf heterogeneity, *Geophysical Research Letters*, 44, 4186–4194, 2017.

Christmann, J., Müller, R., Webber, K. G., Isaia, D., Schader, F. H., Kipfstuhl, S., Freitag, J., and Humbert, A.: Measurement of the fracture 310 toughness of polycrystalline bubbly ice from an Antarctic ice core, *Earth System Science Data*, 7, 87–92, 2015.

Clayton, T., Duddu, R., Hageman, T., and Martínez-Pañeda, E.: The influence of firn layer material properties on surface crevasse propagation in glaciers and ice shelves, *The Cryosphere*, 18, 5573–5593, 2024.

Cook, S., Galton-Fenzi, B. K., Ligtenberg, S. R., and Coleman, R.: Brief communication: widespread potential for seawater infiltration on Antarctic ice shelves, *The Cryosphere*, 12, 3853–3859, 2018.

315 Craw, L., McCormack, F. S., Cook, S., Roberts, J., and Treverrow, A.: Modelling the influence of marine ice on the dynamics of an idealised ice shelf, *Journal of Glaciology*, 69, 342–352, 2023.

Cruz, C. and Lipovsky, B. P.: Fracturing during freezing in salty ice: preliminary analysis using a low-cost model system, 2025.

Cullen, D. and Baker, I.: Observation of impurities in ice, *Microscopy Research and Technique*, 55, 198–207, 2001.

De Rydt, J., Gudmundsson, G. H., Nagler, T., and Wuite, J.: Calving cycle of the Brunt Ice Shelf, Antarctica, driven by changes in ice shelf 320 geometry, *The Cryosphere*, 13, 2771–2787, 2019.

Dempsey, J. P.: The fracture toughness of ice, in: *Ice-Structure Interaction: IUTAM/IAHR Symposium St. John's, Newfoundland Canada 1989*, pp. 109–145, Springer, 1991.

Dutrieux, P., De Rydt, J., Jenkins, A., Holland, P. R., Ha, H. K., Lee, S. H., Steig, E. J., Ding, Q., Abrahamsen, E. P., and Schröder, M.: Strong sensitivity of Pine Island ice-shelf melting to climatic variability, *Science*, 343, 174–178, 2014.

325 Foster, T. D. and Carmack, E. C.: Temperature and salinity structure in the Weddell Sea, *Journal of Physical Oceanography*, 6, 36–44, 1976.

Fricker, H., Bassis, J., Minster, B., and MacAyeal, D.: ICESat's new perspective on ice shelf rifts: The vertical dimension, *Geophysical Research Letters*, 32, 2005a.

Fricker, H., Young, N., Coleman, R., Bassis, J., and Minster, J.-B.: Multi-year monitoring of rift propagation on the Amery Ice Shelf, East Antarctica, *Geophysical Research Letters*, 32, 2005b.

330 Glasser, N. and Scambos, T. A.: A structural glaciological analysis of the 2002 Larsen B ice-shelf collapse, *Journal of Glaciology*, 54, 3–16, 2008.



Grima, C., Greenbaum, J. S., Lopez Garcia, E. J., Soderlund, K. M., Rosales, A., Blankenship, D. D., and Young, D. A.: Radar detection of the brine extent at McMurdo Ice Shelf, Antarctica, and its control by snow accumulation, *Geophysical Research Letters*, 43, 7011–7018, 2016.

335 Gudmundsson, G. H., Paolo, F. S., Adusumilli, S., and Fricker, H. A.: Instantaneous Antarctic ice sheet mass loss driven by thinning ice shelves, *Geophysical Research Letters*, 46, 13 903–13 909, 2019.

Hubbard, B., Luckman, A., Ashmore, D. W., Bevan, S., Kulessa, B., Kuipers Munneke, P., Philippe, M., Jansen, D., Booth, A., Sevestre, H., et al.: Massive subsurface ice formed by refreezing of ice-shelf melt ponds, *Nature communications*, 7, 11 897, 2016.

340 Huth, A., Duddu, R., Smith, B., and Sergienko, O.: Simulating the processes controlling ice-shelf rift paths using damage mechanics, *Journal of Glaciology*, 69, 1915–1928, 2023.

Jacobs, S. S., Helmer, H., Doake, C. S., Jenkins, A., and Frolich, R. M.: Melting of ice shelves and the mass balance of Antarctica, *Journal of Glaciology*, 38, 375–387, 1992.

345 Killingbeck, S. F., Kulessa, B., Miles, K. E., Hubbard, B., Luckman, A., Thompson, S. S., Jones, G., and Galton-Fenzi, B. K.: Imaging brine infiltration and basal marine ice in Larsen C Ice Shelf, Antarctic Peninsula, from borehole measurements and transient electromagnetics, *Geophysical Research Letters*, 52, e2025GL115 908, 2025.

King, E. C., De Rydt, J., and Gudmundsson, G. H.: The internal structure of the Brunt Ice Shelf from ice-penetrating radar analysis and implications for ice shelf fracture, *The Cryosphere*, 12, 3361–3372, 2018.

Kittel, C., Amory, C., Agosta, C., Jourdain, N. C., Hofer, S., Delhasse, A., Doutreloup, S., Huot, P.-V., Lang, C., Fichefet, T., et al.: Diverging future surface mass balance between the Antarctic ice shelves and grounded ice sheet, *The Cryosphere Discussions*, 2020, 1–29, 2020.

350 Krug, J., Weiss, J., Gagliardini, O., and Durand, G.: Combining damage and fracture mechanics to model calving, *The Cryosphere*, 8, 2101–2117, 2014.

Kulessa, B., Booth, A. D., O’Leary, M., McGrath, D., King, E. C., Luckman, A. J., Holland, P. R., Jansen, D., Bevan, S. L., Thompson, S. S., et al.: Seawater softening of suture zones inhibits fracture propagation in Antarctic ice shelves, *Nature Communications*, 10, 5491, 2019.

355 Kuruppu, M. D., Obara, Y., Ayatollahi, M. R., Chong, K., and Funatsu, T.: ISRM-suggested method for determining the mode I static fracture toughness using semi-circular bend specimen, *Rock Mechanics and Rock Engineering*, 47, 267–274, 2014.

Larour, E., Rignot, E., and Aubry, D.: Modelling of rift propagation on Ronne Ice Shelf, Antarctica, and sensitivity to climate change, *Geophysical research letters*, 31, 2004.

Lewis, E.: The practical salinity scale 1978 and its antecedents, *IEEE Journal of Oceanic Engineering*, 5, 3–8, 1980.

360 Lipovsky, B. P.: Ice shelf rift propagation and the mechanics of wave-induced fracture, *Journal of Geophysical Research: Oceans*, 123, 4014–4033, 2018.

Lipovsky, B. P.: Ice shelf rift propagation: stability, three-dimensional effects, and the role of marginal weakening, *The Cryosphere*, 14, 1673–1683, 2020.

Marsh, O., Arthern, R., and De Rydt, J.: Ocean tides trigger ice shelf rift growth and calving, *Nature Communications*, 16, 6697, 2025.

365 Marsh, O. J., Luckman, A. J., and Hodgson, D. A.: Brief communication: Rapid acceleration of the Brunt Ice Shelf after calving of iceberg A-81, *The Cryosphere*, 18, 705–710, 2024.

Miles, B., Stokes, C., Jenkins, A., Jordan, J., Jamieson, S., and Gudmundsson, G.: Intermittent structural weakening and acceleration of the Thwaites Glacier Tongue between 2000 and 2018, *Journal of Glaciology*, 66, 485–495, 2020.

Mulvaney, R., Bremner, S., Tait, A., and Audley, N.: A medium-depth ice core drill, *Memoirs of National Institute of Polar Research. Special issue*, 56, 82–90, 2002.



370 Naughten, K. A., Holland, P. R., and De Rydt, J.: Unavoidable future increase in West Antarctic ice-shelf melting over the twenty-first century, *Nature Climate Change*, 13, 1222–1228, 2023.

Nicola, L., Notz, D., and Winkelmann, R.: Revisiting temperature sensitivity: how does Antarctic precipitation change with temperature?, *The Cryosphere*, 17, 2563–2583, 2023.

Nixon, W. and Schulson, E.: A micromechanical view of the fracture toughness of ice, *Le Journal de Physique Colloques*, 48, C1–313, 1987.

375 Noël, B., Van Wessem, J. M., Wouters, B., Trusel, L., Lhermitte, S., and Van Den Broeke, M. R.: Higher Antarctic ice sheet accumulation and surface melt rates revealed at 2 km resolution, *Nature communications*, 14, 7949, 2023.

Orr, A., Deb, P., Clem, K. R., Gilbert, E., Bromwich, D. H., Boberg, F., Colwell, S., Hansen, N., Lazzara, M. A., Mooney, P. A., et al.: Characteristics of surface “melt potential” over Antarctic ice shelves based on regional atmospheric model simulations of summer air temperature extremes from 1979/80 to 2018/19, *Journal of Climate*, 36, 3357–3383, 2023.

380 Pralong, A. and Funk, M.: Dynamic damage model of crevasse opening and application to glacier calving, *Journal of Geophysical Research: Solid Earth*, 110, 2005.

Pritchard, H., Ligtenberg, S. R., Fricker, H. A., Vaughan, D. G., van den Broeke, M. R., and Padman, L.: Antarctic ice-sheet loss driven by basal melting of ice shelves, *Nature*, 484, 502–505, 2012.

Reed, B., Green, J. M., Jenkins, A., and Gudmundsson, G. H.: Melt sensitivity of irreversible retreat of Pine Island Glacier, *The Cryosphere*, 385 18, 4567–4587, 2024.

Rist, M., Sammonds, P., Murrell, S., Meredith, P., Oerter, H., and Doake, C.: Experimental fracture and mechanical properties of Antarctic ice: preliminary results, *Annals of glaciology*, 23, 284–292, 1996.

Rist, M., Sammonds, P., Oerter, H., and Doake, C.: Fracture of Antarctic shelf ice, *Journal of Geophysical Research: Solid Earth*, 107, ECV–2, 2002.

390 Scambos, T., Fricker, H. A., Liu, C.-C., Bohlander, J., Fastook, J., Sargent, A., Massom, R., and Wu, A.-M.: Ice shelf disintegration by plate bending and hydro-fracture: Satellite observations and model results of the 2008 Wilkins ice shelf break-ups, *Earth and Planetary Science Letters*, 280, 51–60, 2009.

Scambos, T. A., Bohlander, J., Shuman, C. A., and Skvarca, P.: Glacier acceleration and thinning after ice shelf collapse in the Larsen B embayment, Antarctica, *Geophysical Research Letters*, 31, 2004.

395 Schulson, E. M.: Brittle failure of ice, *Engineering fracture mechanics*, 68, 1839–1887, 2001.

Schulson, E. M. and Duval, P.: Creep and fracture of ice, Cambridge university press, 2009.

Timco, G. W. and Frederking, R. M. W.: Flexural strength and fracture toughness of sea ice, *Cold Regions Science and Technology*, 8, 35–41, 1983.

Van der Veen, C.: Fracture mechanics approach to penetration of surface crevasses on glaciers, *Cold Regions Science and Technology*, 27, 400 31–47, 1998.

van der Veen, C. J.: Fracture mechanics approach to penetration of bottom crevasses on glaciers, *Cold Regions Science and Technology*, 27, 213–223, [https://doi.org/10.1016/S0165-232X\(98\)00006-8](https://doi.org/10.1016/S0165-232X(98)00006-8), 1998.

Walker, C., Bassis, J., Fricker, H., and Czerwinski, R.: Structural and environmental controls on Antarctic ice shelf rift propagation inferred from satellite monitoring, *Journal of Geophysical Research: Earth Surface*, 118, 2354–2364, 2013.

405 Weeks, W.: *On sea ice*, University of Alaska Press, 2010.

Weiss, J.: Subcritical crack propagation as a mechanism of crevasse formation and iceberg calving, *Journal of Glaciology*, 50, 109–115, 2004.



Wille, J. D., Favier, V., Jourdain, N. C., Kittel, C., Turton, J. V., Agosta, C., Gorodetskaya, I. V., Picard, G., Codron, F., Santos, C. L.-D., et al.: Intense atmospheric rivers can weaken ice shelf stability at the Antarctic Peninsula, *Communications Earth & Environment*, 3, 90, 410 2022.